Incoherent J/ψ electroproduction from the deuteron at energies available at Jefferson Laboratory and the elastic J/ψ-nucleon scattering amplitude

Gary T. Howell and Gerald A. Miller

Department of Physics, University of Washington, Seattle, Washington 98195-1560, USA
(Received 19 March 2013; published 17 July 2013)

Calculations are presented for incoherent J/ψ electroproduction from the deuteron at Jefferson Laboratory energies, including the effects of J/ψ-nucleon rescattering in the final state, in order to determine the feasibility of measuring the J/ψ-nucleon scattering length, or the J/ψ-nucleon scattering amplitude at lower relative energies than in previous measurements. It is shown that for a scattering length of the size predicted by existing theoretical calculations, it would not be possible to determine the scattering length. However, it may be possible to determine the scattering amplitude at significantly lower relative energies than the only previous measurements.

I. INTRODUCTION

With the upcoming 12-GeV upgrade at Jefferson Laboratory (JLab), electroproduction of the J/ψ at JLab on a proton or deuteron will be possible. With the mass of the J/ψ being 3.097 GeV, the threshold virtual photon energy for electroproduction (at small Q^2) on a single nucleon is $\nu_{\rm thresh} \simeq 8.2$ GeV in the LAB frame, and is thus accessible with a 12-GeV electron beam. Most of the existing data on J/ψ photoproduction and electroproduction is at much higher energy. The 12-GeV upgrade provides the opportunity to measure J/ψ production near threshold [1]. In addition, measuring electroproduction on the deuteron provides the opportunity to measure the J/ψ-nucleon elastic scattering amplitude at lower energies than previous measurements, if the rescattering of the produced J/ψ on the spectator nucleon in the deuteron is non-negligible. This paper presents calculations of the incoherent J/ψ production amplitude from the deuteron near threshold (in order to determine if the J/ψ-nucleon scattering length can be determined) and at somewhat higher energy where the J/ψ-nucleon scattering amplitude may be determined. We use a model that takes into account quasielastic production from the deuteron (with production on one nucleon while the spectator nucleon recoils freely) as well as rescattering effects in the final state (proton-neutron rescattering and J/ψ-nucleon rescattering).

The motivation for the work in the first part of this paper (Secs. II–IV) was a proposal at JLab [2] to measure the J/ψ-nucleon scattering length by the reaction $\gamma^* + d \rightarrow J/\psi + p + n$. The proposed experiment would detect the outgoing proton and the decay products (e^+e^-) of the J/ψ, for a kinematically complete measurement. The reason the J/ψ-nucleon scattering length is of interest is that several authors have argued that a nuclear bound state of the J/ψ may exist [3,4]. They propose that the force between a J/ψ and a nucleon is purely gluonic in nature, and therefore is the analog in QCD of the van der Waals force in electrodynamics, since the hadrons are color neutral objects. There is very little experimental data on elastic J/ψ-nucleon scattering. There has only been one experimental measurement of it, at SLAC in 1977, where the J/ψ-nucleon total cross section was extracted by measuring production of J/ψ on nuclei and using an optical model for the rescattering of the J/ψ on the spectator nucleons [5].

Measurement of the scattering length provides information on the bound states of the two particles involved in the scattering. In particular, for an attractive potential, if the scattering length is positive then there exists a bound state. Theoretical calculations of the J/ψ-nucleon scattering length [3,4,6,7] predict a scattering length too small to produce a J/ψ-nucleon bound state. However, it would be large enough that there could exist a nucleus-J/ψ bound state in a large enough nucleus. Since the scattering length is the negative of the zero-energy scattering amplitude, in order to measure this it is necessary for the two particles to scatter with small relative momentum. In the case of $\gamma^* + d \rightarrow J/\psi + p + n$ at the energies that are kinematically allowed in the proposed JLab experiment, it is not possible to have an on-mass-shell nucleon and J/ψ scatter at small relative momentum. For an incident virtual photon of energy $\nu = 9$ GeV, and an outgoing J/ψ-neutron pair with zero relative momentum, the minimum possible momentum of the neutron in the LAB frame (deuteron at rest) is $\simeq 0.85$ GeV; for $\nu = 6.5$ GeV and zero relative momentum of the J/ψ-neutron pair, the minimum LAB momentum of the neutron is $\simeq 1$ GeV. For zero relative momentum of the outgoing pair, the initial LAB momentum of an on-shell neutron in the deuteron (before the collision with the J/ψ) must equal the final LAB momentum of the neutron. Therefore, the momentum of the neutron inside the deuteron would have to be 0.85 GeV (for $\nu = 9$ GeV). However, the deuteron wave function at that momentum is very small (essentially zero).

So although the proposed experiment [2] may not be able to measure the J/ψ-nucleon scattering length, it might still be possible to measure the on-mass-shell J/ψ-nucleon scattering amplitude, but at higher relative energies. The relative energy of the J/ψ-neutron pair would still be significantly smaller than in the only existing data (from the 1977 experiment at SLAC). Under certain kinematic conditions, the dominant contributions to the amplitude will come from proton-neutron (p-n) rescattering and/or J/ψ-n rescattering after the J/ψ is produced. If we fix the magnitude of the outgoing neutron's momentum at a moderately large value (here taken to be

0.5 GeV) the contribution of the impulse diagram (where the J/ψ is produced on the proton and the neutron recoils freely) will be negligible, since the impulse diagram is proportional to the value of the deuteron wave function at that momentum. This higher-energy rescattering is the subject of the second part of this paper (Sec. V).

This paper is organized as follows. Section II reviews the general expression for the cross section of electroproduction from a nucleus. In Sec. III the kinematics for the case of zero and small relative momentum of the outgoing J/ψ-neutron pair is discussed. In Sec. IV the calculation of the invariant amplitudes for $\gamma^* + D \rightarrow J/\psi + p + n$ are presented, including the one-loop diagrams corresponding to the p-n and J/ψ-nucleon rescattering processes. In order to calculate the amplitude corresponding to the low-energy J/ψ-neutron scattering, which involves the scattering length, model J/ψ-neutron scattering wave functions and potentials are used, and it is shown that the resulting amplitude is insensitive to the model used. In addition, it is shown that for the kinematic conditions of the JLab experiment, the dominant amplitude is the impulse diagram, corresponding to J/ψ production on the neutron with the proton recoiling freely, with no rescattering of any particles. This demonstrates that the measurement of the J/ψ-nucleon scattering length is not feasible for the JLab experiment. Finally, in Sec. V calculations of the amplitude for $\gamma^* + D \rightarrow J/\psi + p + n$ are presented under different kinematic conditions (not restricting the outgoing J/ψ-neutron pair to small relative momentum). There it is shown that if the J/ψ-neutron elastic scattering amplitude is somewhat larger than the value measured at SLAC at higher energy, it may be possible to extract this amplitude from the JLab experiment.

II. ELECTROPRODUCTION FROM A NUCLEUS

We consider here electron scattering from the deuteron with production of a vector meson, with the final state of the proton-neutron system being a continuum state. The formalism for the cross section for electroproduction from a nucleus can be found in Ref. [8]. Here we summarize the relevant facts. We consider here the completely unpolarized electron (initial and final) cross section. Then the cross section can be written in terms of the amplitudes for $\gamma^* + d \rightarrow p + n + V$, i.e., vector meson production from virtual photons. In the LAB frame, with ϵ' the final electron energy, Ω' the final electron solid angle, Ω_V the vector meson solid angle, and $\mathbf{p}_{pn}^*$ the final proton-neutron relative momentum in the p-n center-of-mass frame, the eightfold differential cross section has the form

$$\frac{d^8\sigma}{d\epsilon' d\Omega' d\Omega_V d^3 p_{pn}^*}$$
$$= (\text{kinematic factors})$$
$$\times \left(v_T R_{fi}^T + v_{TT} R_{fi}^{TT} + v_L R_{fi}^L + v_{TL} R_{fi}^{TL} \right), \quad (1)$$

where the factors

$$R_{fi}^T = |\langle f|J_{+1}(\mathbf{q})|i\rangle|^2 + |\langle f|J_{-1}(\mathbf{q})|i\rangle|^2, \quad (2)$$

$$R_{fi}^{TT} = 2\mathrm{Re}\langle f|J_{+1}^*(\mathbf{q})|i\rangle\langle f|J_{-1}(\mathbf{q})|i\rangle, \quad (3)$$

$$R_{fi}^{TL} = -2\mathrm{Re}\langle f|\rho^*(\mathbf{q})|i\rangle(\langle f|J_{+1}(\mathbf{q})|i\rangle - \langle f|J_{-1}(\mathbf{q})|i\rangle), \quad (4)$$

$$R_{fi}^L = |\langle f|\rho(\mathbf{q})|i\rangle|^2, \quad (5)$$

are in terms of the matrix elements of the spherical vector components of the electromagnetic current operator J between the initial deuteron state $|i\rangle$ and final hadron $(p + n + J/\psi)$ state $|f\rangle$. v_T, v_{TT}, etc., are kinematic factors that only depend on the electron momenta. R_{fi}^T is the sum of the squares of the amplitudes for $\gamma^* + d \rightarrow p + n + V$ for transversely polarized virtual photons, whereas R_{fi}^{TT} is an interference term between these two amplitudes. R_{fi}^L is the square of the amplitude for a longitudinally polarized virtual photon, while R_{fi}^{TL} is an interference term between the amplitudes for production from transverse and longitudinally polarized photons. The matrix element R_{fi}^{TL} is proportional to $\cos\phi$, while R_{fi}^{TT} is proportional to $\cos 2\phi$, where ϕ is the angle between the plane including the initial and final electron momenta, and the plane including the three-momentum transfer $\mathbf{q}$ and the J/ψ momentum $\mathbf{p}_V$. Thus if we integrate the cross section over ϕ, the terms R^{TT} and R^{TL} drop out. Or, if we assume helicity conservation (i.e., the helicity of the outgoing J/ψ is equal to the helicity of the photon) then $R^{TT} = R^{TL} = 0$. Moreover, several theoretical models [11,12] indicate that for small Q^2, the amplitude for J/ψ electroproduction from transverse virtual photons is much larger than the amplitude for production from longitudinally polarized virtual photons; for $Q^2 = 0$ (photoproduction) the production amplitude for longitudinal photon polarization is of course exactly zero. Therefore in what follows we will neglect R_{fi}^L, and so the differential cross section is simply given by R_{fi}^T multiplied by kinematic factors. Thus our task is to calculate

$$R_{fi}^T = |\langle f|J_{+1}(\mathbf{q})|i\rangle|^2 + |\langle f|J_{-1}(\mathbf{q})|i\rangle|^2 \equiv |F_+|^2 + |F_-|^2, \quad (6)$$

where $F_\pm$ are the amplitudes for J/ψ production from positive and negative helicity virtual photons. In the following we will calculate the amplitude for $\gamma^* + d \rightarrow p + n + V$ by evaluating Feynman diagrams corresponding to the various processes contributing to it.

III. KINEMATICS FOR SMALL J/ψ-NEUTRON RELATIVE MOMENTUM

We will assume kinematics where the outgoing J/ψ and neutron have a small relative momentum. Since the scattering length is the zero-energy limit of the scattering amplitude, in order to measure it the relative momentum of the $J/\psi - n$ system must be small. An estimate of how small can be obtained by requiring only S-wave scattering, meaning the contribution of higher partial waves should be negligible. The classical relation between impact parameter and angular momentum yields an estimate for the maximum l that contributes. If the relative momentum of the $J/\psi - n$ pair is p^* and the impact parameter is b, then the orbital angular momentum in the $J/\psi - n$ c.m. frame is $L \simeq p^* b = b\sqrt{2\mu T^*}$ where T^* is the total kinetic energy in the two-body c.m. frame and μ is the reduced mass. The largest angular momentum
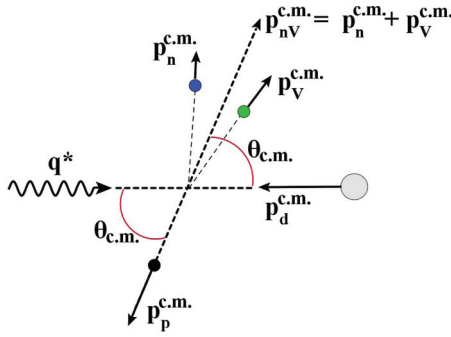
FIG. 1. (Color online) Momenta and angles in the overall c.m. frame, for coplanar kinematics.

partial wave that will be scattered is obtained by setting b equal to the range of the potential. With $L^2 = l(l + 1)$ (we take $\hbar = 1$), the condition for only S-wave scattering is that $l \ll 1$, which implies $L^2 = b^2 2\mu T^* \ll 1$. Taking the range of the interaction to be $\simeq 1$ fm yields $T^* \ll 30$ MeV.

Experimentally, perhaps the simplest quantity to measure is the total production cross section, integrated over all available phase space, for a given incident photon energy. However, if we restrict the photon energy such that the maximum J/ψ-neutron c.m. kinetic energy $T^*_{\max}$ is small in of all the available phase space, then that means that the maximum proton-neutron relative energy will also be small everywhere in the available phase space: for a given value of the Mandlestam variable s for a system consisting of three particles, the total kinetic energy of any two of the particles (say 1 and 2) in their c.m. frame satisfies

$$T^*_{12} \leqslant \sqrt{s} - m_1 - m_2 - m_3. \qquad (7)$$

The low-energy $J/\psi - n$ scattering amplitude is expected to be much smaller than the low-energy $p - n$ scattering amplitude, and therefore the $p - n$ rescattering would dominate over the $J/\psi - n$ rescattering, as contributions to the total production cross section. Thus we need to restrict our considerations to a kinematic range where the $p - n$ rescattering is at relatively high energy, while the $J/\psi - n$ rescattering is at very low energy, in order to have the possibility that the $J/\psi - n$ rescattering makes a noticeable contribution to the differential cross section.

The ideal situation would be to have the final J/ψ and neutron sitting at rest in the LAB, with the proton moving off at high velocity. Such a final state is kinematically allowed for other reactions, e.g., $\pi^+ d \rightarrow \eta pp$, $\gamma^* d \rightarrow \eta pn$, but it is not possible for the reaction $\gamma^* d \rightarrow J/\psi \, pn$, for any real or virtual photon four-momentum.

Figure 2 shows the minimum possible outgoing neutron LAB momentum and the corresponding proton LAB momentum vs $\theta_{\mathrm{c.m.}}$ for fixed $T^*_{\mathrm{V}n} = 30$ MeV (see Fig. 1 for the definition of $\theta_{\mathrm{c.m.}}$); graphs are shown for photon LAB energy $\nu = 9$ GeV and for $\nu = 6.5$ GeV. One can see that the neutron's momentum is always greater than at least 0.6 GeV. Since the maximum nucleon momentum in the deuteron is around 0.3 GeV (the deuteron momentum-space wave function is negligible for momenta larger than that) that means that in order for these final-state kinematics to occur, the neutron must have acquired its large momentum through a scattering event. In fact it will turn out that the dominant process corresponds to the impulse approximation wherein the J/ψ is produced on the neutron itself, and the proton simply recoils freely. For the kinematics of interest here, rescattering processes (e.g., J/ψ-neutron rescattering, J/ψ-proton rescattering, proton-neutron rescattering) make very small contributions to the total amplitude.

We use the following notation throughout this paper: $q = (\nu, \mathbf{q})$ is the virtual photon four-momentum in the LAB, with $q^2 = -Q^2 < 0$; $\mathbf{p}_p$ is the outgoing proton LAB three-momentum; $\mathbf{p}_n$ is the outgoing neutron LAB three-momentum; $\mathbf{p}_V$ is the J/ψ LAB three-momentum; and the same variables with c.m. superscripts denote their values in the overall (three-body) center-of-mass frame. θ_p, θ_n, and θ_V denote the angle that the outgoing proton, neutron, and J/ψ momenta, respectively, make with $\mathbf{q}$, in the LAB frame.

IV. INVARIANT SCATTERING AMPLITUDES

The Feynman diagrams considered here are shown in Figs. 3 and 4. There are three diagrams for production on the proton, and three similar diagrams where the J/ψ is produced on the neutron. In all cases we are interested in kinematics where the J/ψ and neutron have small relative momentum. The diagrams are covariant, and hence give Lorentz invariant amplitudes. In the diagrams, $\mathcal{M}^{\gamma V}$ is the Lorentz invariant
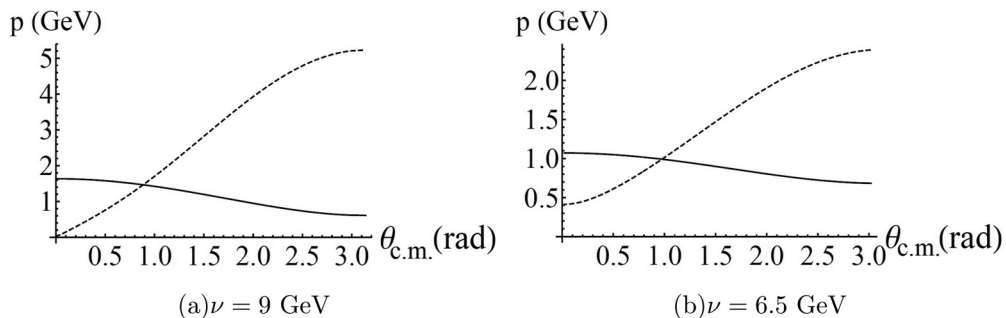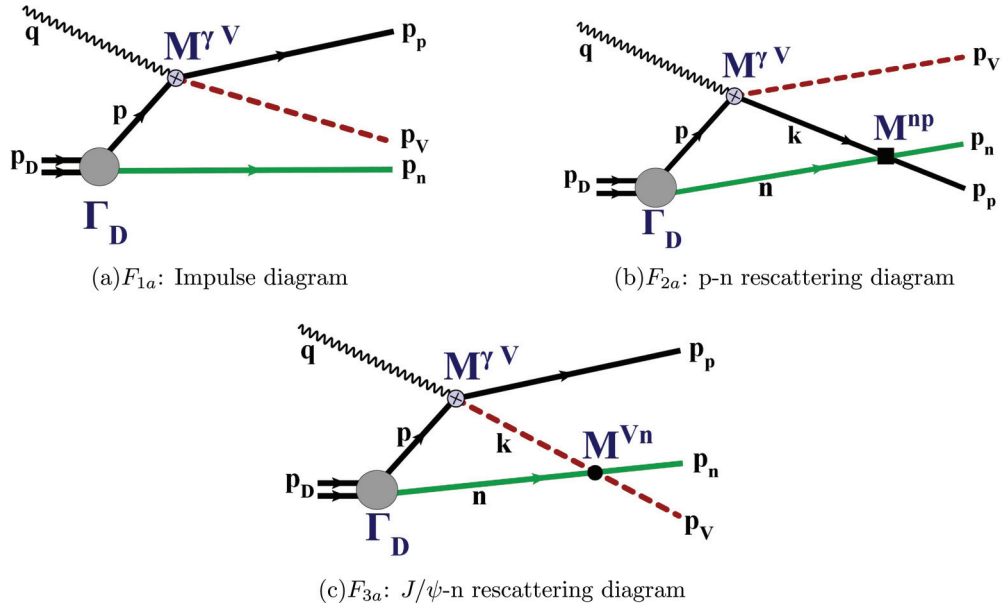

FIG. 2. Minimum possible neutron LAB momentum (solid curve), and the corresponding proton LAB momentum (dashed curve), vs. $\theta_{\mathrm{c.m.}}$, for $T^*_{\mathrm{V}n} = 30$ MeV and two values of photon LAB energy ν.

(a)F_{1a}: Impulse diagram

(b)F_{2a}: p-n rescattering diagram

(c)F_{3a}: J/ψ-n rescattering diagram

FIG. 3. (Color online) Feynman diagrams for $\gamma^* + d \to J/\psi + p + n$, for production on the proton.

amplitude for the quasi-two-body process $\gamma^* + N \to V + N$ (where N is a nucleon, and V stands for the J/ψ), while $\mathcal{M}^{Vn}$ is the Lorentz invariant amplitude for the elastic scattering process $V + n \to V + n$ (with n meaning neutron), and $\mathcal{M}^{Vp}$ and $\mathcal{M}^{np}$ are the same for elastic J/ψ-proton scattering and neutron-proton scattering, respectively.
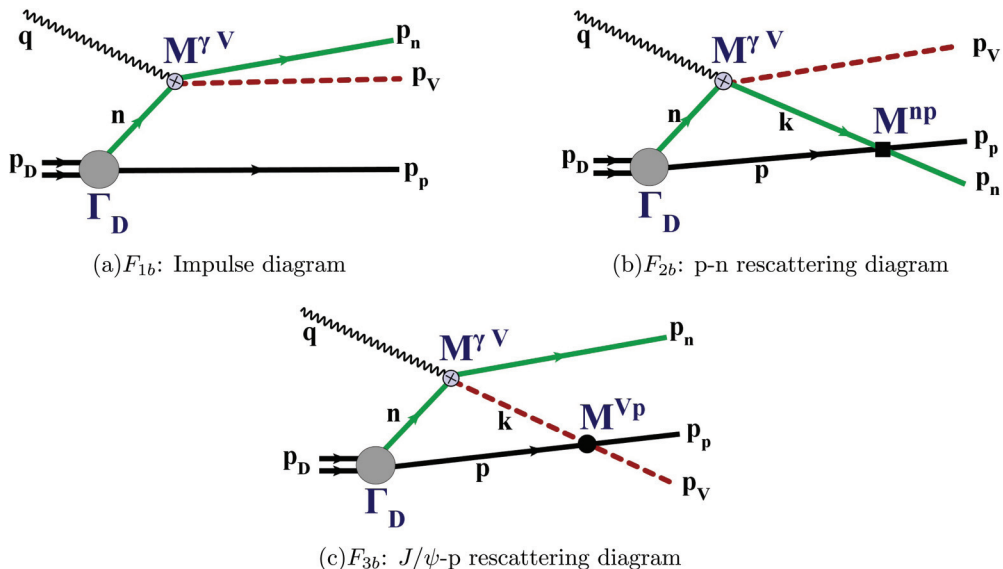
A. Impulse diagrams

Amplitudes F_{1a} and F_{1b} are the impulse diagrams, where the J/ψ is produced on one of the nucleons and the other nucleon (the "spectator") recoils freely without interacting with the other particles. In F_{1a} the vector meson is produced

on the proton and the neutron is the spectator, while in F_{1b} the production occurs on the neutron and the proton is the spectator. The invariant amplitudes in this case are

$$F_{1a} = \mathcal{M}^{\gamma V}(s_{1a}, t_{1a}) \frac{\Gamma_D(p)}{D(p)} \qquad (8)$$

$$F_{1b} = \mathcal{M}^{\gamma V}(s_{1b}, t_{1b}) \frac{\Gamma_D(n)}{D(n)}. \qquad (9)$$

Here $\mathcal{M}^{\gamma V}$ is the Lorentz invariant amplitude for the quasi-two-body process $\gamma^* + N \to V + N$ (where N is a nucleon, and V stands for the J/ψ), Γ_D is the covariant vertex function for the virtual dissociation $D \to p + n$, and $D(p)$ is the propagator denominator for the intermediate-state

(a)F_{1b}: Impulse diagram

(b)F_{2b}: p-n rescattering diagram

(c)F_{3b}: J/ψ-p rescattering diagram

FIG. 4. (Color online) Feynman diagrams for $\gamma^* + d \to J/\psi + p + n$, for production on the neutron.

nucleon, $D(p) \equiv -p^2 + m^2 - i\epsilon$. s_{1a}, t_{1a}, s_{1b}, and t_{1b} are the Mandelstam variables for the two-body production process $\gamma^* + N \to V + N$. Evaluated in the LAB frame, and neglecting any contributions to the deuteron vertex from antinucleons, the deuteron vertex function is related to the nonrelativistic deuteron wave function by [13]

$$\psi_D(\mathbf{k}_{\rm rel}) = \frac{-\Gamma_D(p)}{\sqrt{2p^0(2\pi)^3} \, D(p)}, \qquad (10)$$

where in the LAB frame, $\mathbf{k}_{\rm rel} = \mathbf{p} = -\mathbf{p}_n$ for F_{1a}, and $\mathbf{k}_{\rm rel} = \mathbf{p}_p = -\mathbf{n}$ for F_{1b} ($\mathbf{k}_{\rm rel}$ is the proton's momentum inside the deuteron, in the LAB frame, for both). In terms of the deuteron wave function, the amplitudes are

$$F_{1a} = -\mathcal{M}^{\gamma V}(s_{1a}, t_{1a}) \, \psi_D(-\mathbf{p}_n)\sqrt{2m(2\pi)^3} \qquad (11)$$

$$F_{1b} = -\mathcal{M}^{\gamma V}(s_{1b}, t_{1b}) \, \psi_D(\mathbf{p}_p)\sqrt{2m(2\pi)^3}. \qquad (12)$$

The amplitudes $\mathcal{M}^{\gamma V}$ used in calculations are to be taken from experimental data on J/ψ production on a single nucleon; we assume here that the amplitudes for production from a neutron is the same as for production from a proton.

In the above expressions for the amplitudes F_{1a} and F_{1b}, spin labels have been suppressed. The initial virtual photon and the deuteron are in specific spin states, the final hadrons are in specific spin states, and there is a sum over the spin states of the intermediate-state virtual nucleon. For example, the amplitude F_{1b}, including spin state specification, is explicitly

$$F_{1b} = -\sqrt{2m(2\pi)^3} \sum_{m_1} \mathcal{M}^{\gamma V}(m_1, \lambda, m_n, \lambda_V)$$
$$\times \psi_D^M(\mathbf{p}_p, m_1, m_p), \qquad (13)$$

where m_1 is the spin state of the intermediate-state neutron (i.e., the line with momentum n in the Feynman diagram), m_n and m_p are the spin states of the final neutron and proton, λ is the photon polarization, λ_V is the J/ψ polarization, and M is the deuteron spin state. In what follows we will assume that the two-body amplitudes for spin flip are negligible compared to the non-spin-flip amplitudes, and so the amplitudes are diagonal in the nucleon spin, and also in the photon and J/ψ spin. In that case we are able to calculate the spin-averaged squares of the various amplitudes F_{1a}, F_{2a}, etc., and the spin-averaged square of the total amplitude. We have included the contribution from the D state in the deuteron wave function. For $\nu = 9$ GeV the D state was found to not make a significant contribution to the amplitudes, but for $\nu = 6.5$ GeV the D state did contribute significantly, especially for the impulse diagram F_{1b}. The deuteron wave function used was the Argonne $v18$ wave function.

All two-body amplitudes $\mathcal{M}^{\gamma V}$, $\mathcal{M}$ are related to the corresponding two-body differential cross section by

$$\frac{d\sigma}{dt} = \frac{1}{16\pi \lambda(s, m_1^2, m_2^2)} |\mathcal{M}|^2, \qquad (14)$$

where the flux factor λ is given in terms of the incident particle masses m_1 and m_2 by

$$\lambda(s, m_1^2, m_2^2) = (s - m_1^2 - m_2^2)^2 - 4m_1^2 m_2^2, \qquad (15)$$

and s and t are the Mandelstam variables for the two-body process.

1. Parameterization of the amplitudes $\mathcal{M}^{\gamma V}$

If the cross section for J/ψ production on a single nucleon is parametrized as

$$\frac{d\sigma}{dt} = A_1 e^{B_1 t}, \qquad (16)$$

with the parameters A_1, B_1 dependent on energy (in principle), then the elementary production amplitude $\mathcal{M}^{\gamma V}$ is given by

$$\mathcal{M}^{\gamma V} = -i \sqrt{16\pi A_1 \lambda(s, -Q^2, m^2)} e^{\frac{1}{2}B_1 t}, \qquad (17)$$

where s and t are either s_{1a}, t_{1a} or s_{1b}, t_{1b}.

The parameters A_1 and B_1 that are needed for the elementary J/ψ production amplitude $\mathcal{M}^{\gamma V}$ were estimated from the (scant) existing data on exclusive J/ψ production on a nucleon. The only available data for the incident photon energy $\nu \simeq 10$ GeV is from a photoproduction experiment at Cornell in 1975 [14]. For ν in the range 9.3 to 10.4 GeV, they determined $A_1 = 1.1 \pm 0.17$ nb/GeV$^2 = (2.8 \pm 0.43) \times 10^{-6}$ GeV^{-4} and $B_1 = 1.31 \pm 0.19$ GeV^{-2}. Those are the values used in this analysis.

2. F_{1a} and F_{1b}

Since F_{1a} is proportional to $\Psi(\mathbf{p}_n)$, and as seen in Fig. 2 the outgoing neutron's momentum is always greater than $\simeq 0.6$ GeV, the amplitude F_{1a} will therefore be very small, since the deuteron wave function is negligible for those values of momentum. The amplitude F_{1b}, on the other hand, is proportional to $\Psi(\mathbf{p}_p)$; thus as seen in Fig. 2 for $\theta_{\rm c.m.} < 0.3$ rad F_{1b} should be non-negligible since the proton momentum is less than 0.4 GeV over that range of $\theta_{\rm c.m.}$.

B. One-loop diagrams

The covariant expression for a general one-loop diagram (see Fig. 5) is

$$F = -\int \frac{d^4 n}{i(2\pi)^4} \frac{\Gamma(n')}{D(n')} \frac{\mathcal{M}^{\gamma V}\mathcal{M}}{D(n)D(k)}, \qquad (18)$$
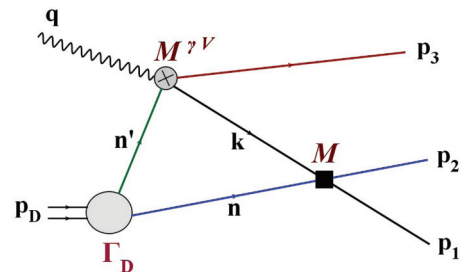

FIG. 5. (Color online) General one-loop diagram. n and p_2 are the same particle (either neutron or proton). The line n can be either a proton or a neutron.

where n', n, k are the internal four-momenta indicated in the figure, $\mathcal{M}$ stands for either $\mathcal{M}^{pn}$, $\mathcal{M}^{Vn}$, or $\mathcal{M}^{Vp}$ (elastic scattering amplitude for proton-neutron, V-neutron, or V-proton scattering, respectively), and $D(p) = p^2 - m_p^2 + i\epsilon$, etc., are propagator denominators. Spin labels have been suppressed in Eq. (18); in particular, there is an implicit sum over the spin states of the intermediate-state particles (the lines labeled n, k, and n'). There are four diagrams total for a given set of outgoing proton, neutron and J/ψ momenta. Taking $\mathbf{p}_2 = \mathbf{p}_n$, $\mathbf{p}_1 = \mathbf{p}_p$ (so that the internal line n is the neutron, and n' and k are the proton) gives one diagram ($p-n$ rescattering diagram). The other three are: $\mathbf{p}_2 = \mathbf{p}_n$, $\mathbf{p}_1 = \mathbf{p}_V$, where the internal line n is the neutron, k is the J/ψ, and n' and p_3 are the proton ($V-n$ rescattering diagram); $\mathbf{p}_2 = \mathbf{p}_p$, $\mathbf{p}_1 = \mathbf{p}_n$, where the internal line n is the proton, and n' and k are the neutron (another $p-n$ rescattering diagram); and $\mathbf{p}_2 = \mathbf{p}_p$, $\mathbf{p}_1 = \mathbf{p}_V$, where the internal line n is the proton, k is the J/ψ, and n' and p_3 are the neutron ($V-p$ rescattering diagram).

All of the one-loop diagrams can be evaluated in the same manner. We follow closely the method of [9]. We first integrate over n^0 by taking the positive-energy pole at $n^0 = \omega_n - i\epsilon$, where $\omega_n = \sqrt{m^2 + \mathbf{n}^2}$, coming from the propagator denominator $D(n)$. This corresponds to neglecting antinucleon components of the deuteron wave function. We also use the relation Eq. (10) (and we work in the rest frame of the deuteron). This gives

$$F = \sqrt{\frac{2m}{(2\pi)^3}} \int \frac{d^3 n}{2\omega_n} \Psi(\mathbf{n}) \frac{\mathcal{M}^{\gamma V}\mathcal{M}}{D(k)}. \quad (19)$$

Note that in this expression, the internal nucleon line n is now on-mass-shell, since $n^0 = \omega_n$. Thus in the time-ordered diagram of Fig. 5, only the lines n' and k can be off-shell; all the rest are on-shell.

The above expression for the amplitude F can be separated into two terms, one term in which the line k is on-mass-shell and one in which k is off-mass-shell, by using the relation

$$\frac{1}{x + i\epsilon} = -i\pi\delta(x) + \mathcal{P}\frac{1}{x} \quad (20)$$

for the remaining propagator in Eq. (19) (with $\mathcal{P}$ representing the principal value) and by choosing the coordinate system shown in Fig. 6 where the n_z axis is along the direction of the vector $\mathbf{p}_{12} \equiv \mathbf{p}_1 + \mathbf{p}_2$. The δ function term gives the on-mass-shell part of the amplitude, and the principal value term gives the off-mass-shell part. This separation is useful since the elementary amplitudes $\mathcal{M}^{\gamma V}$, $\mathcal{M}$ can be determined (at least
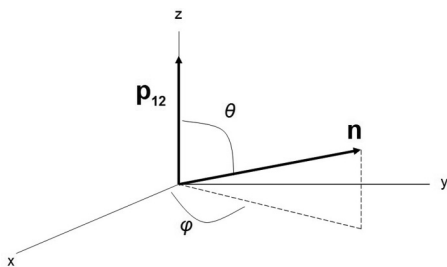

FIG. 6. Coordinate system used. For the on-shell amplitude, θ is fixed for a given $n \equiv |\mathbf{n}|$ and $\mathbf{p}_1$, $\mathbf{p}_2$.

in principle) directly from experimental data on the relevant two-body scattering processes only when all four particles involved (two initial and two final) are on-mass-shell. This is not the case if one of the particles involved is off-mass-shell. But if for reasonable choices of the off-mass-shell amplitudes the off-mass-shell part is small compared to the on-shell part, then the off-mass-shell part will not play an important role. The result for the on-shell and off-shell parts of the one-loop amplitude is [9]

$$F = F^{on} + F^{off}, \quad (21)$$

where

$$F^{on} = -i\pi \frac{1}{\sqrt{2m(2\pi)^3}} \frac{1}{2|\mathbf{p}_{12}|}$$
$$\times \int_0^{2\pi} d\phi \int_{|n_-|}^{n_+} dn\, n\, \Psi(n) \mathcal{M}^{\gamma V}\mathcal{M} \quad (22)$$

and

$$F^{off} = \frac{1}{\sqrt{2m(2\pi)^3}} \frac{1}{2|\mathbf{p}_{12}|} \int_0^{2\pi} d\phi \int_0^{\infty} dn\, n\, \Psi(n)$$
$$\times \mathcal{P} \int d\cos\theta \frac{\mathcal{M}^{\gamma V}\mathcal{M}}{f_{12}(n) + \cos\theta}. \quad (23)$$

Here

$$f_{12}(n) \equiv \frac{s_{12} + m^2 - m_k^2 - 2E_{12}\omega_n}{2n\,|\mathbf{p}_{12}|}, \quad (24)$$

with $n \equiv |\mathbf{n}|$. $s_{12} \equiv (p_1 + p_2)^2$ is the Mandelstam s variable for the elastic scattering of particles 1 and 2, m_k is the mass of the real particle, which the line k represents, $E_{12} \equiv E_1 + E_2$, and θ is as shown in Fig. 6. Note that f_{12} is independent of θ and ϕ.

In the amplitude F^{on}, the limits of integration $|n_-|$ and n_+ are the solutions of

$$f_{12}(n_\pm)^2 = 1, \quad (25)$$

which are

$$n_\pm = \frac{E_2^*}{\sqrt{s_{12}}}|\mathbf{p}_{12}| \pm \frac{p_2^*}{\sqrt{s_{12}}}E_{12}, \quad (26)$$

where p_2^*, E_2^* are the momentum and energy of outgoing particle 2 in the c.m. frame of particles 1 and 2, and particle 2 is the same particle as the internal line with momentum $\mathbf{n}$. The range of n given by $|n_-| \leqslant n \leqslant n_+$ is the range of n for which it is kinematically possible for the line k to be on-mass-shell (given that n, p_1, and p_2 are on-shell). In F^{on} the value of $\cos\theta$ is fixed at

$$\cos\theta = -f_{12}(n) = -\frac{s_{12} + m^2 - m_k^2 - 2E_{12}\omega_n}{2|\mathbf{p}_{12}|n}. \quad (27)$$

The amplitudes $\mathcal{M}^{\gamma V}$, $\mathcal{M}$ in F^{on} are evaluated, for a given n and ϕ, at this value of $\cos\theta$. The amplitude $\mathcal{M}$ in F^{on} is fully on-shell, i.e., all four particle lines n, k, p_1, and p_2 are on-mass-shell. The amplitude $\mathcal{M}^{\gamma V}$ has only one particle off-shell (n'), but given that the magnitude of $\mathbf{n}$ is small (due to the deuteron wave function), n' is almost on-shell: $n'^0 = M_d - \omega_n \simeq M_d - m \simeq m$, and so $(n')^2 = m^2 + \mathcal{O}(\frac{n^2}{m^2})$.
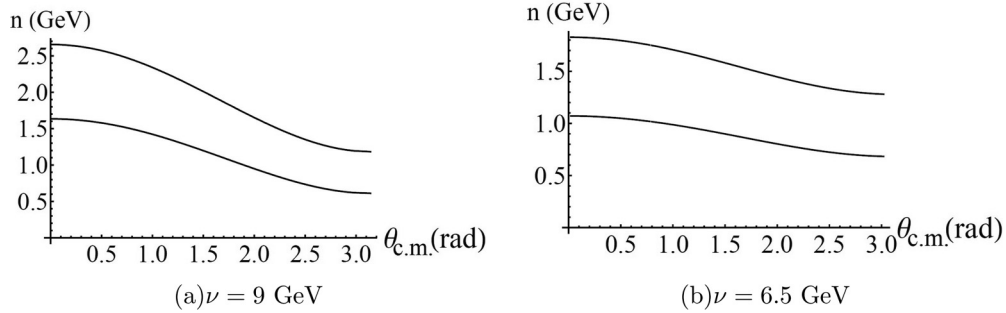
FIG. 7. $n_\pm$ vs $\theta_{\text{c.m.}}$ for the amplitude F_{3a} (J/ψ-neutron rescattering), for $T_{\text{Vn}}^* = 30$ MeV, and $\nu = 9.0$ GeV and $\nu = 6.5$ GeV. Upper curve is n_+, lower curve is n_-.

In the amplitude F^{off}, k is never on-mass-shell; the principal value imposes this, since for k to be on-mass-shell, $\cos\theta$ must equal $-f_{12}(n)$, which never occurs in the principal value. Thus the amplitudes $\mathcal{M}^{\gamma V}$, $\mathcal{M}$ that enter into F^{off} have either one particle off-mass-shell (for $\mathcal{M}$) or two particles off-shell (for $\mathcal{M}^{\gamma V}$). In our calculations the amplitude F^{off} was much smaller than F^{on}, for any of the Feynman diagrams in Fig. 3 and 4 (except for F_{3a}), for the kinematics considered here, and for reasonable expressions for the off-shell amplitudes $\mathcal{M}^{\gamma V}$, $\mathcal{M}$.

C. General features of the one-loop diagrams

Inspection of Eq. (22) shows that a necessary condition for the on-shell part of a given one-loop diagram to be non-negligible is that the corresponding $|n_-|$ must be small enough so that the range of integration in Eq. (22) includes the momenta where the deuteron wave function is significant. Since n_- depends on the final-state kinematics [Eq. (26)], graphs of n_- as a function of one of the final state variables reveal regions where the on-shell amplitude can be significant, and regions where it will be negligible.

For the diagram of most interest, F_{3a}, particles 1 and 2 are the J/ψ and neutron, respectively. Fig. 7(a) shows $n_\pm$ vs. $\theta_{\text{c.m.}}$ for $T_{\text{Vn}}^* = 30$ MeV, for $\nu = 9$ GeV, and Fig. 7(b) shows the same for $\nu = 6.5$ GeV, for the diagram F_{3a}. At both of these photon energies, n_- is greater than ~ 0.6 GeV for all $\theta_{\text{c.m.}}$, and so the on-shell amplitude will be negligible since the deuteron wave function is negligible for that momentum.

For the amplitudes F_{2a}, F_{2b}, and F_{3b}, the corresponding n_- graphs are shown in Fig. 9 for $\nu = 9$ GeV and $\nu = 6.5$ GeV, for $T_{\text{Vn}}^* = 30$ MeV. Note that at a given value of $\theta_{\text{c.m.}}$ and T_{Vn}^*, the neutron LAB momentum can range from a minimum to a maximum allowed value (with these two values both corresponding to $\mathbf{p}_n$ and $\mathbf{p}_V$ pointing in the same direction in the LAB, with $\theta' = 0$ in Fig. 8), and the values of n_- for F_{2a}, F_{2b}, and F_{3b} depend on the neutron LAB momentum in addition to $\theta_{\text{c.m.}}$ and T_{Vn}^*. For our calculations, we have fixed the neutron LAB momentum for a given $\theta_{\text{c.m.}}$ (and $T_{\text{Vn}}^* = 30$ MeV) at its minimum value; we denote this value by $p_{n,\text{min}}$. One can see from these graphs that for $\nu = 9$ GeV, there are intervals of the variable $\theta_{\text{c.m.}}$ for which the on-shell parts of F_{2a}, F_{2b}, and F_{3b} should be non-negligible, since $n_- < 0.05$ GeV there

(note that for the diagram F_{3b}, the J/ψ-proton rescattering occurs at relatively high energy, if the J/ψ-neutron relative energy is small; so F_{3b} is not directly related to the J/ψ-nucleon scattering length). For $\nu = 6.5$ GeV, n_- is larger than $\simeq 0.4$ GeV, and so these on-shell amplitudes should be small. This is borne out by the exact calculations, where the one-loop on-shell amplitudes for $\nu = 6.5$ GeV are in general much smaller than those for $\nu = 9$ GeV.

D. Parameters used in the elementary two-body amplitudes

For the calculation of the amplitudes, using Eq. (22) and Eq. (23), the elementary amplitudes $\mathcal{M}^{\gamma V}$ and $\mathcal{M}$ are phenomenological amplitudes obtained from existing experimental data, related to the two-body cross section by Eq. (14). We take the individual two-body differential cross sections to be of the form

$$\frac{d\sigma}{dt} = A e^{Bt}, \tag{28}$$

where A and B can depend on energy. Thus we have

$$\mathcal{M} = -i\sqrt{16\pi\lambda(s, m_1^2, m_2^2)A}\, e^{\frac{1}{2}Bt}, \tag{29}$$

relating $\mathcal{M}$ to A and B.

The values of A and B depend on the relative momentum (or energy) of the rescattering pair. Table I lists the values of the momentum p of the neutron in the proton's rest frame
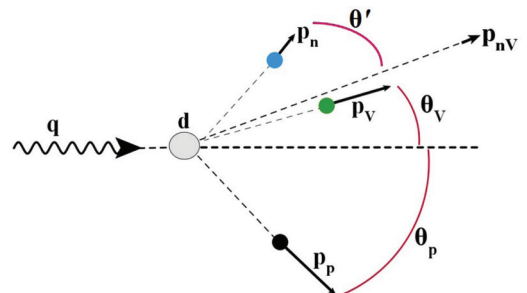

FIG. 8. (Color online) LAB frame momenta. For a given $\theta_{\text{c.m.}}$ and T_{Vn}^*, the neutron LAB momentum can range between a minimum and maximum value, both of which correspond to $\theta' = 0$ in the figure. $\mathbf{p}_{nV} = \mathbf{p}_V + \mathbf{p}_n$.
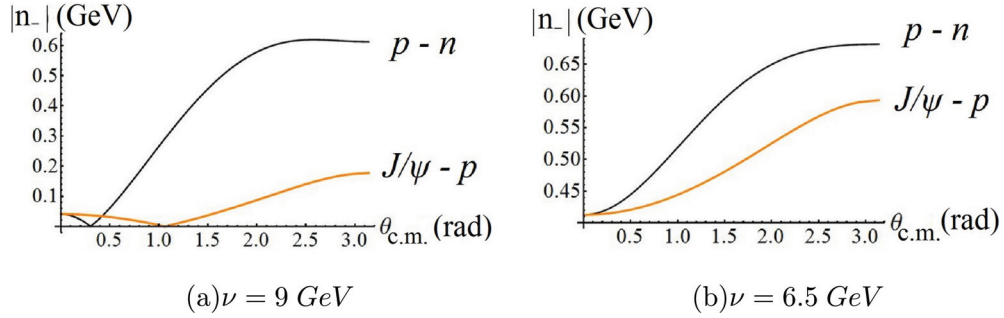
FIG. 9. (Color online) n_- vs $\theta_{c.m.}$ for proton-neutron rescattering and J/ψ-proton rescattering amplitudes, for $T^*_{Vn} = 30$ MeV, $p_n = p_{n,\min}$.

(for the $p-n$ subsystem) and the momentum p of the J/ψ in the proton's rest frame (for the $V-p$ subsystem), for the case of $T^*_{Vn} = 0$. Note that these quantities are independent of $\theta_{c.m.}$ (easily shown in the overall c.m. frame). Also given in Table I is the total kinetic energy of the pair in the c.m. frame of that pair, T^*_{12}. Given the values of the momentum p, we can determine the parameters that enter into the elementary amplitudes $\mathcal{M}^{pn}$, $\mathcal{M}^{Vp}$.

1. $p-n$ scattering parameters

For $\nu = 9$ GeV, the existing data [10] for $p-n$ scattering at incident momentum $p = 2.25$ GeV gives $B_{pn} = 5.7\ to\ 6.2$ GeV^{-2}. The value of A_{pn} can be obtained from the total $p-n$ cross section by using the optical theorem and neglecting the real part of the scattering amplitude

$$\frac{d\sigma}{dt}\Big|_{t=0} = \frac{1}{16\pi}\sigma^2_{tot} = A_{pn} \qquad (30)$$

The measured value of σ_{tot} given in the table is then used to calculate A_{pn}. For $\nu = 6.5$ GeV, the existing data for $p-n$ scattering at momentum $p = 0.86$ GeV gives $B_{pn} = 6.9$ GeV^{-2} [10] and $A_{pn} = 160$ GeV^{-4} [15].

2. $J/\psi - p$ scattering parameters

There is very little data on elastic J/ψ-proton scattering from which to determine the parameters A_{Vp} and B_{Vp} that are needed for the J/ψ-proton rescattering amplitude M^{Vp}. For the present analysis, we have assumed that the t-slope for elastic J/ψ-nucleon scattering is equal to the t slope for the process $\gamma^* + N \rightarrow J/\psi + N$, and so we have taken $B_{Vp} = B_{\gamma V} = 1.31 \pm 0.19$ GeV^{-2}. We can obtain A_{Vp} from the total J/ψ-nucleon cross section, using the optical theorem; however, there has only been one measurement of $\sigma^{J/\psi\ N}_{tot}$ [17].

In an experiment in 1977 at SLAC [5] J/ψ photoproduction was measured on beryllium and tantalum targets, and the total J/ψ-nucleon cross section was extracted by using an optical model for the rescattering of the produced J/ψ from the other nucleons in the nucleus. The value they obtained was $\sigma^{J/\psi\ N}_{tot} = 3.5 \pm 0.8$ mb, which gives via the optical theorem $A_{Vp} = 1.61 \pm 0.4$ GeV^{-4}. In that paper, however, they also note that the measured J/ψ-photoproduction cross section together with vector meson dominance arguments would give a J/ψ-nucleon total cross section of $\simeq 1$ mb. So we can assume the value of the J/ψ-nucleon total cross section to be not very well known. In addition, the photon energy in the SLAC experiment was 20 GeV, and so assuming forward production of the J/ψ, then the energy of the J/ψ in the LAB frame would also be $\simeq 20$ GeV, giving a kinetic energy in the LAB of $\simeq 17$ GeV. This is significantly larger than the kinetic energy of the J/ψ in the proton rest frame considered here, where for $\nu = 9$ GeV it is 4.94 GeV and for $\nu = 6.5$ GeV it is 1.1 GeV. This introduces more uncertainty in the value of A_{Vp} to be used. In Ref. [4], a theoretical calculation of the J/ψ-nucleon scattering length yields a value for the total J/ψ-nucleon cross section at threshold of 7 mb, and it is argued that the total cross section should decrease as the energy is increased from threshold. Thus at the energy of the J/ψ-proton rescattering here, the value of A_{Vp} may be larger than the value measured in the experiment at SLAC. For the purpose of calculating the amplitude F_{3b}, however, we will use the value measured at SLAC.

3. Subthreshold J/ψ production

The threshold photon energy for production on a single nucleon at rest is

$$\nu_{thresh} = m_V + \frac{m_V^2 + Q^2}{2m} \qquad (31)$$

TABLE I. Parameters used in elementary scattering amplitudes.

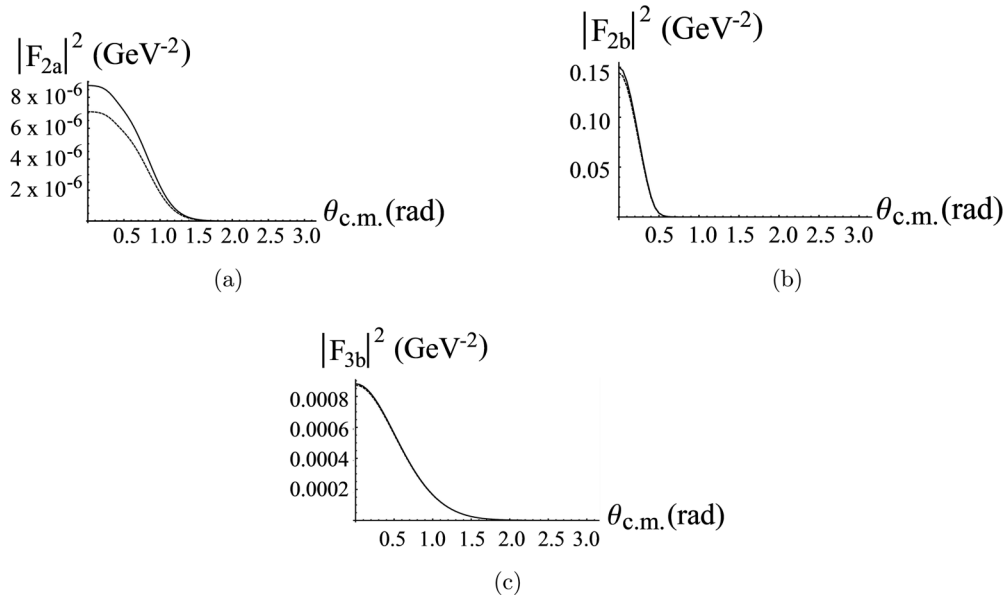| ν (GeV)	Subsystem	p (GeV)	T^*_{12} (GeV)	B (GeV^{-2})	σ_{tot} (mb)	A (GeV^{-4})
9	$n-p$	2.25	0.64	5.7–6.2	43–46	260
9	$V-p$	7.4	1.02	1.31	3.5	1.61
6.5	$n-p$	0.86	0.16	6.9	35	160
6.5	$V-p$	2.84	0.247	1.31	3.5	1.61

FIG. 10. Squares of amplitudes for $\nu = 9.0$ GeV, $T^*_{\mathrm{Vn}} = 30$ MeV, $p_n = p_{n,\min}$. The solid curve is the total (on-shell plus off-shell parts), while the dashed curve is only including the on-shell part of the amplitude.

while for production on the deuteron it is

$$\nu_{\mathrm{thresh}} = m_V + \frac{m_V^2 + Q^2}{2M_d} \qquad (32)$$

For $Q^2 = 0.5$ GeV, these are 8.47 GeV and 5.78 GeV, respectively.

For $\nu = 6.5$ GeV, which is below threshold for J/ψ production on a single nucleon at rest, we assume that the production mechanism is the same as for production on a free nucleon. The Fermi motion of the nucleon in the deuteron is what allows the production to occur, i.e., if the nucleon is moving towards the photon with a large enough momentum then the value of $s_1 = (q + p)^2$, where p is the four-momentum of the nucleon in the deuteron, will be above the threshold value. In the calculation of the amplitudes for $\nu = 6.5$ GeV this condition was imposed on the internal nucleon momentum in the integrals involved.

E. Calculated on-shell and off-shell amplitudes

Using the parameters in Table I, the on-shell and off-shell parts of the amplitudes were calculated. The squares of the individual amplitudes F_{2a}, F_{2b}, and F_{3b} are shown in Figs. 10 and 11; shown in the graphs is a curve, which includes only the (square of the) on-shell part of the amplitude, and also a curve which is the square of the total amplitudes including both the on-shell and off-shell parts. For the off-shell parts, the same parametrizations of the elementary amplitudes $\mathcal{M}^{\gamma V}$ and $\mathcal{M}$ were used as for the on-shell parts. As stated previously, the off-shell parts are very small compared to the on-shell parts, which means that knowledge of the exact forms of the off-shell elementary amplitudes $\mathcal{M}^{\gamma V}$ and $\mathcal{M}$ are not needed.

Since the J/ψ-nucleon scattering length is expected to be small (much smaller than, e.g., the proton-neutron scattering length), the J/ψ-neutron rescattering diagram F_{3a} should be

a small contribution to the total amplitude. This is borne out in the next subsection, where F_{3a} is calculated using a model potential and wave function, for a value of the scattering length on the order of that predicted by theoretical models.

F. J/ψ-neutron rescattering diagrams and the scattering length

Diagram F_{3a} [Fig. 3(c)] is the J/ψ-neutron rescattering diagram. This is the diagram where the J/ψ and neutron scatter from each other with small relative momentum; hence this amplitude will involve the scattering length for the J/ψ-neutron interaction.

For this diagram, we have $\mathbf{p}_{12} = \mathbf{p}_{\mathrm{Vn}} \equiv \mathbf{p}_V + \mathbf{p}_n$ in Eqs. (22)–(27), and θ is the angle between $\mathbf{p}_{\mathrm{Vn}}$ and $\mathbf{n}$ (see Fig. 6). For $T^* = 0$, where $T^* = T^*_n + T^*_V$ (* indicates the c.m. frame of the $V-n$ system), we have $n_+ = |n_-|$ [see Eq. (26)], and so $F^{\mathrm{on}}_{3a} = 0$. For small T^* (below, e.g., 100 MeV), F^{on}_{3a} will be small because $n_- \gtrsim 0.45$ GeV for the possible JLab kinematics (see Fig. 7). Thus the main contribution to F_{3a} is from F^{off}_{3a}, for which the intermediate-state J/ψ is always off-mass-shell. However, because of the propagator denominator $f_{12}(n) + \cos\theta$, where

$$f_{12}(n) + \cos\theta = \frac{1}{2|\mathbf{p}_{\mathrm{Vn}}|n} \left(k^2 - m_V^2\right), \qquad (33)$$

contributions to F^{off}_{3a} from values of $\mathbf{n}$ for which k is far off-mass-shell will be small. To obtain estimates of F^{off}_{3a}, we will therefore evaluate it using on-mass-shell values of $\mathcal{M}^{\gamma V}$ and $\mathcal{M}^{\mathrm{Vn}}$.

The relation between the invariant amplitude $\mathcal{M}^{\mathrm{Vn}}$ and the scattering amplitude $f(k, \theta)$ is [16]

$$\mathcal{M} = -8\pi \sqrt{s_{\mathrm{Vn}}} \, f(k, \theta) \qquad (34)$$

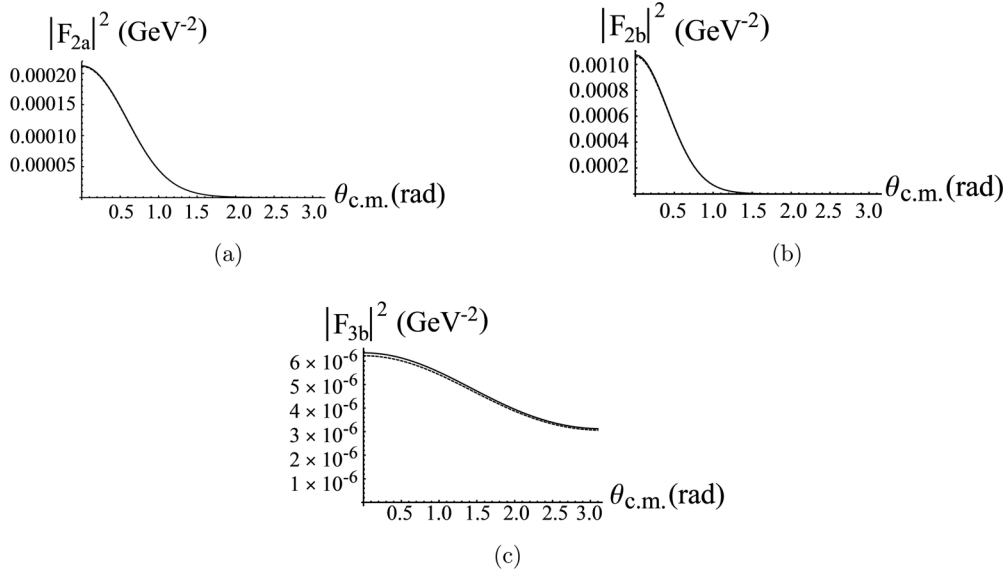for the on-energy-shell amplitudes. The half-off-energy shell amplitudes are related in the same way.

FIG. 11. Squares of amplitudes for $\nu = 6.5$ GeV, $T_{Vn}^* = 30$ MeV, $p_n = p_{n,\min}$. The solid curve is the total (on-shell plus off-shell parts), while the dashed curve is only including the on-shell part of the amplitude.

Our normalization conventions are the following. The scattering length a is given by

$$\lim_{k \to 0} f(k, \theta) = -a. \tag{35}$$

The off-energy-shell amplitude is given by

$$
\begin{aligned}
f^{Vn}(\mathbf{k}_1, \mathbf{k}_2) &= -(2\pi)^2 \mu \langle \mathbf{k}_2 | V | \Psi_{\mathbf{k}_1}^{(+)} \rangle \\
&= -(2\pi)^2 \mu \langle \Psi_{\mathbf{k}_2}^{(-)} | V | \mathbf{k}_1 \rangle \\
&= -(2\pi)^2 \mu \langle \mathbf{k}_1 | V | \Psi_{\mathbf{k}_2}^{(-)} \rangle^*,
\end{aligned}
\tag{36}
$$

where V is the potential, μ is the reduced mass, $\mathbf{k}_1$ is the initial relative momentum [in terms of $\mathbf{n}$, $\mathbf{k}$ in Fig. 3(c)], $\mathbf{k}_2$ is the final relative momentum [in terms of $\mathbf{p}_V$, $\mathbf{p}_n$ in Fig. 3(c)], and $\Psi_{\mathbf{k}_2}$ is the exact scattering wave function for asymptotic relative momentum $\mathbf{k}_2$. Since this off-energy-shell scattering amplitude depends on the scattering wave function $\Psi_{\mathbf{k}_2}^{(-)}$ and the potential V, both of which are unknown for J/ψ-nucleon elastic scattering, we will resort to models in order to estimate the amplitude.

We normalize our S-wave scattering wave function $\Psi_{\mathbf{k}}$, and define the radial wave function $u(r)$, by

$$\Psi_{\mathbf{k}}(r) = \frac{1}{\sqrt{(2\pi)^3}} e^{i\delta(k)} \frac{u(r)}{r}, \tag{37}$$

where $\delta(k)$ is the S-wave phase shift. In order to calculate the matrix element, we will specify a model zero-energy wave function $u_0(r)$, which determines the potential $V(r)$ via the Schrödinger equation, and use that potential to solve for the wave function for $k \neq 0$ (the subscript zero on u_0 indicates it is for $k = 0$).

We assume the J/ψ-nucleon potential is of finite range, and so is zero for r larger than some distance R. The phase-shift $\delta(k)$ satisfies the following well-known properties as $k \to 0$:

(i) for a repulsive potential, or an attractive potential that doesn't admit a bound state: $\delta \to -ak$ as $k \to 0$;

(ii) for an attractive potential which admits a single bound state: $\delta \to \pi - ak$ as $k \to 0$

The zero-energy wave function $\Psi_0(r)$ outside the range of the potential is then

$$\Psi_0^{out}(r) = \frac{1}{\sqrt{(2\pi)^3}} e^{i\delta(0)} \frac{u_0^{out}(r)}{r} = \frac{1}{\sqrt{(2\pi)^3}} \frac{r-a}{r} \tag{38}$$

for both cases, while the zero-energy radial wave function u_0^{out} differs by a minus sign for the two cases; this is purely due to including the factor $e^{i\delta(k)}$ in the definition of Ψ_k in Eq. (37). Our normalization conventions give $a > 0$ for either a repulsive potential or an attractive potential with a bound state, and $a < 0$ for an attractive potential that doesn't admit a bound state. In all cases a is the intercept on the r axis of $u_{out}^0(r)$.

Theoretical calculations [4,6] give values of $|a| \simeq 0.3$ fm, with effective range $r_e \simeq 2.0$ fm. It is thought that the potential is attractive, but too weak to support a bound state. Below, calculations of F_{3a} are made for both cases of an attractive potential: $a > 0$ (bound state) and $a < 0$ (no bound state).

G. Positive scattering length a

For the case of a positive scattering length and attractive potential (which possesses a bound state), we have $u_0^{out}(r) = -(r-a)$. We choose the simplest zero-energy wave function $u_0(r)$ consistent with the standard continuity requirements on $u(r)$ at $r = 0$ and $r = R$ required by the Schrödinger equation. This yields

$$u_0^{in}(r) = \left(-1 + \frac{3a}{R} \right) r + \left(-\frac{3a}{R^2} \right) r^2 + \left(\frac{a}{R^3} \right) r^3. \tag{39}$$

One further requirement on u_0^{in} is that u_0^{in} have no zeros on the interval $[0, R]$ (besides at $r = 0$). This ensures that the corresponding potential $V(r)$ is nonsingular, since for $k = 0$,

(a) Squares of individual amplitudes, for positive scattering length a. Dashed curve is the square of the total amplitude. $V - p$: F_{3b}; $V - n$: F_{3a}; $p - n$: F_{2b}.

(b) Electroproduction differential cross-section (logarithmic scale).

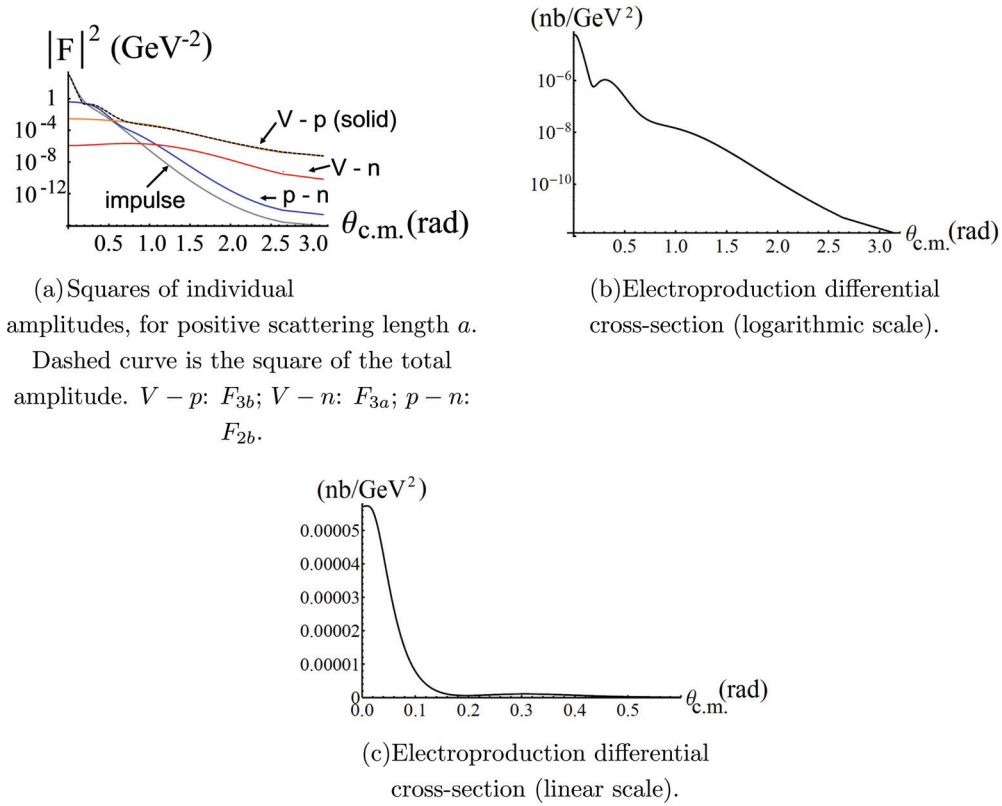(c) Electroproduction differential cross-section (linear scale).

FIG. 12. (Color online) Squares of amplitudes, and electroproduction differential cross section Eq. (47), for $\nu = 9$ GeV, $T_{Vn}^* = 30$ MeV, $p_n = p_{n,\min}$. The solid curves in (b) and (c) include all amplitudes, while the dashed curves (which are not distinguishable from the solid curve) omit F_{3a} for both positive and negative scattering length a, for the model potential of Eq. (43).

$V(r) = \frac{1}{2\mu} \frac{u''}{u}$. The zeros of u_0^{in} are at $r = 0$ and

$$\frac{r}{R} = \frac{3}{2} \pm \frac{1}{2} \sqrt{4 \frac{R}{a} - 3} \tag{40}$$

and the right-hand side must lie outside the range $[0, 1]$. This requires either

$$R < a \tag{41}$$

or

$$R > 3a. \tag{42}$$

The potential is

$$V(r) = \frac{1}{2\mu} \frac{1}{r} \frac{r - R}{R^2 \left(3 - \frac{R}{a}\right) - 3Rr + r^2} \tag{43}$$

and one can see that for $R > 3a$ the potential is repulsive. Therefore we require $R < a$.

1. Model wave function for $k \neq 0$

Given this model potential we can proceed to calculate the off-shell scattering amplitude Eq. (36) and the amplitude F_{3a}^{off} once we calculate the wave function u for nonzero k for a given a and R. Taking $a = 0.3$ fm, $R = 0.1$ fm, and solving the Schrödinger equation for $k < 100$ MeV numerically, we find that the wave function $\Psi_k(r)$ and the off-shell amplitude

$f(p, k)$ depend very weakly on k over the entire momentum range from $k = 0$ to $k = 100$ MeV.

Since we are only interested in the J/ψ-neutron relative momentum up to around 100 MeV, it is legitimate to approximate the off-energy-shell amplitude $f^{\text{Vn}}(p, k) \simeq f^{\text{Vn}}(p, 0)$ for the range of k we are interested in. For our model wave function u_0^{in} we can evaluate $f^{\text{Vn}}(p, 0)$ analytically

$$f^{\text{Vn}}(\mathbf{p}, 0) = \frac{-2\pi^2}{\sqrt{(2\pi)^3}} \int d^3 r \, e^{-i\mathbf{p}\cdot\mathbf{r}} U(r) \Psi_0(r)$$
$$= \frac{6a}{p^2 R^2} \left(-1 + \frac{\sin pR}{pR}\right). \tag{44}$$

The momentum p appearing in $f(p, 0)$ is the relative momentum of the J/ψ-neutron pair in their center-of-mass frame, before they scatter in diagram F_{3a}; it is thus the magnitude of $\mathbf{n}$ (or $-\mathbf{k}$) in the outgoing $V - n$ center-of-mass frame, and so we must boost n to that frame.

H. Negative scattering length a

If the potential is attractive but too weak to support a bound state, then $a < 0$ and we have $u_0^{\text{out}}(r) = r - a$. In this case the zero-energy wave function is

$$u_0^{\text{in}} = \left(1 - \frac{3a}{R}\right) r + \left(\frac{3a}{R^2}\right) r^2 - \left(\frac{a}{R^3}\right) r^3. \tag{45}$$

The requirement that u have no zeros on $[0, R]$ imposes no restriction on a and R in this case. Theoretical calculations give a around -0.3 fm, and effective range $r_e \simeq 2.0$ fm [4,6]. Using these values with our model wave function and potential implies $R = 1.3$ fm. Again there is very little variation with k of the wave functions and off-shell amplitudes for k from 0 to 0.1 GeV, so to calculate F_{3a} in this case we will again approximate $f^{Vn}(\mathbf{p}, \mathbf{k}) \simeq f^{Vn}(\mathbf{p}, 0)$. This yields

$$f^{Vn}(\mathbf{p}, 0) = \frac{6a}{p^2 R^2}\left(1 - \frac{\sin pR}{pR}\right). \qquad (46)$$

I. Results

The electroproduction differential cross section in the LAB frame, shown in Figs. 12 and 13, is given by

$$\frac{d^8\sigma}{dE' d\Omega' dp_p d\Omega_p d\Omega_n}$$

$$= \frac{v_0 V_T\ E'}{8(2\pi)^3 M_d\ E}\frac{1}{8(2\pi)^5}\frac{p_p^2}{E_p}\frac{p_n^3}{|E_V\ p_n^2 - E_n\mathbf{p}_n \cdot \mathbf{p}_V|}\ |F|^2 \qquad (47)$$
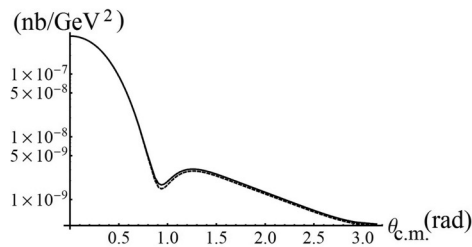
where $F = F_{1a} + F_{1b} + F_{2a} + F_{2b} + F_{3a} + F_{3b}$ is the total amplitude for J/ψ production from a virtual photon, and

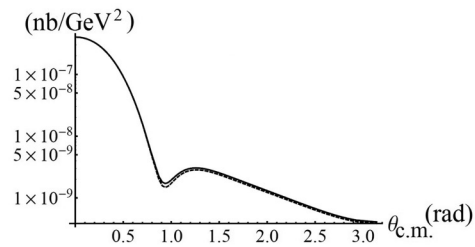$$v_0 = \sqrt{16E^2 E'^2 - Q^4} = 4EE'\cos^2(\theta'/2), \qquad (48)$$

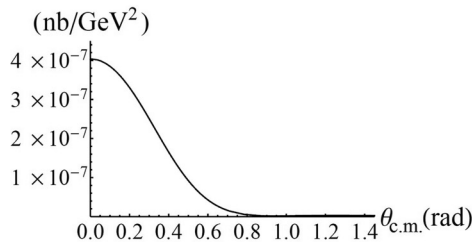$$V_T = \frac{1}{2}\frac{Q^2}{\mathbf{q}^2} + \frac{Q^2}{v_0}, \qquad (49)$$

and

$$E' = E - \nu = 12\ \text{GeV} - \nu. \qquad (50)$$

In the above, E is the initial electron energy (taken to be 12 GeV), E' is the final electron energy, and θ' is the scattering angle of the electron relative to the initial electron momentum (all quantities in the LAB frame).

The results are shown in Figs. 12 and 13. For $\nu = 9$ GeV, the squares of the individual amplitudes F_{1b}, F_{2b}, F_{3b}, and F_{3a} are also shown in Fig. 12(a), along with the square of the total amplitude including all diagrams. As can be seen in that graph, the amplitude F_{3a} makes a negligible contribution to the total amplitude. There are intervals of $\theta_{c.m.}$ where the amplitudes F_{1b}, F_{2b}, and F_{3b} individually dominate the total amplitude. However, by comparing Fig. 12(a) with Fig. 12(c), which shows the electroproduction differential cross section on a linear scale, over the range of $\theta_{c.m.}$ for which the cross section is non-negligible (for $0 < \theta_{c.m.} < 0.2$ rad) the cross section is due exclusively to the impulse diagram F_{1b}. The very small "bump" visible in Fig. 12(c) at $\theta_{c.m.} \simeq 0.3$ rad is due to the proton-neutron rescattering amplitude F_{2b}.

For $\nu = 6.5$ GeV, the difference between the cross section including F_{3a} and omitting F_{3a} is visible in the logarithmic-scale graphs [Figs. 13(a) and 13(b)], but not in the linear-scale graph, Fig. 13(c).

F_{3a} was also calculated using three other potentials: a square-well potential yielding $a = 0.3$ fm and $R = 0.1$ fm, and also the potential of Eq. (43) but with $a = 0.3$ fm, $R = 0.29$ fm, and a square-well potential yielding $a = 0.3$ fm but with $R = 0.29$ fm. There was a negligible difference between the values of F_{3a} calculated with these potentials.

J. Conclusion

It does not appear to be possible to measure the J/ψ-nucleon scattering length via production on the deuteron,

(a)Positive scattering length a. Solid curve includes all amplitudes, dashed is omitting F_{3a}.

(b)Negative scattering length a. Solid curve includes all amplitudes, dashed is omitting F_{3a}.

(c)Same as 13(b), linear scale

FIG. 13. Electroproduction differential cross section Eq. (47) for $\nu = 6.5$ GeV, $T^*_{Vn} = 30$ MeV, $p_n = p_{n,\text{min}}$, and $a = \pm 0.3\ fm$. In (c), the dashed curves (not distinguishable from solid curve) are omitting F_{3a} for both positive and negative a, for the model potential of Eq. (43).
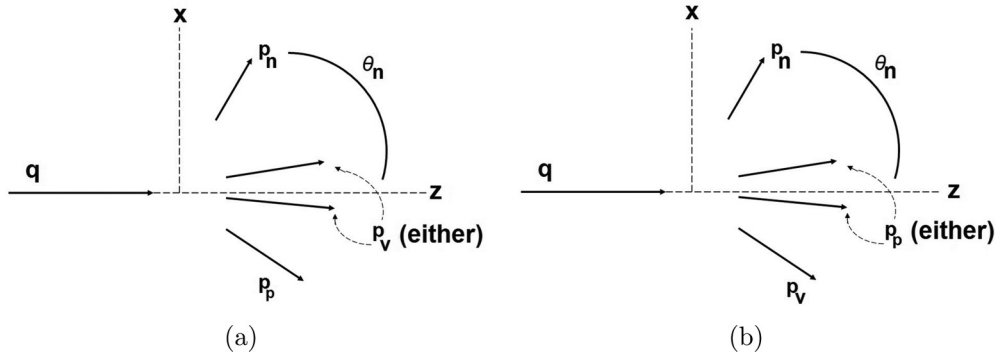
FIG. 14. (a) plus kinematics and (b) minus kinematics. For plus, $\mathbf{p}_p$ is always on the opposite side of the photon momentum $\mathbf{q}$ direction as the neutron momentum. For minus, $\mathbf{p}_V$ is always on the opposite side of the photon momentum $\mathbf{q}$ direction as the neutron momentum.

under the kinematic conditions available at JLab. For small values of the relative momentum of the outgoing J/ψ-neutron pair, the initial momentum of the neutron inside the deuteron that is required for on-mass-shell rescattering of the J/ψ-neutron pair is larger than ~0.6 GeV (see Fig. 7), where the deuteron wave function is negligible. The off-mass-shell part of the rescattering amplitude was calculated using model J/ψ-nucleon potentials and was found to make a negligible contribution to the total amplitude. The vast majority of J/ψ production events, for $T^*_{Vn} \leqslant 0.03$ GeV, will be at small values of $\theta_{c.m.}$, where the impulse diagram F_{1b} dominates, and therefore information on J/ψ-nucleon elastic scattering at small relative energy cannot be obtained.

V. INTERMEDIATE ENERGY J/ψ PRODUCTION ON THE DEUTERON

It may be possible to extract the J/ψ-nucleon elastic scattering amplitude from the $\gamma^* + D \rightarrow J/\psi + p + n$ experiment, at higher relative energy of the J/ψ-nucleon pair, under different kinematic conditions for the final-state particles than was considered in the previous sections of this chapter. Under certain kinematic conditions, the dominant contributions to the amplitude will come from rescattering diagrams ($p-n$ rescattering and $J/\psi-n$ rescattering). If we fix the magnitude of the outgoing neutron's momentum at a moderately large value (here taken to be 0.5 GeV) the contribution of the impulse diagram will be negligible, since the impulse diagram is proportional to the value of the deuteron wave function at that momentum (see Fig. 4 for the impulse and rescattering diagrams). For the analysis presented here, we

  (i) use coplanar kinematics,
 (ii) fix the magnitude of the outgoing neutron momentum at $p_n = 0.5$ GeV,
(iii) fix the four-momentum-transfer-squared $t = (q - p_V)^2$ at a particular value, and
 (iv) plot amplitudes or differential cross sections vs θ_n (the angle that the outgoing neutron momentum $\mathbf{p}_n$ makes with direction of the incoming photon momentum) for fixed p_n and t (see Fig. 14).

For some range of ν and t, these graphs will display peaks due to $p-n$ and $J/\psi-n$ on-mass-shell rescattering. For $\nu = 10$ GeV, the peak due to $J/\psi-n$ rescattering is evident (see Fig. 17), but for $\nu = 9$ GeV it is not evident (see Fig. 18). This analysis is similar to what has been done in Ref. [9] for the reaction $\gamma + D \rightarrow \pi + N + N$.

The kinematics here are very different than in the previous sections. There it was the relative energy of the J/ψ-neutron system that was kept fixed, at a small value, while the parameter that was varied was the production angle of the J/ψ in the overall center-of-mass system.

A. Intermediate-energy J/ψ production

We are interested here in kinematics available at JLab after the 12-GeV upgrade. The maximum (virtual) photon energy is then around 11 GeV. Here we evaluate the amplitude for virtual photon four-momentum $q = (\nu, \mathbf{q})$ with $\nu = 10$ GeV, $Q^2 = -q^2 = 0.5$ GeV, keeping $p_n = 0.5$ GeV and t fixed. The results presented here are for $t = -2$ GeV^2; calculations were done for larger values of $|t|$, with similar results (although the total amplitude decreases with increasing $|t|$). We consider
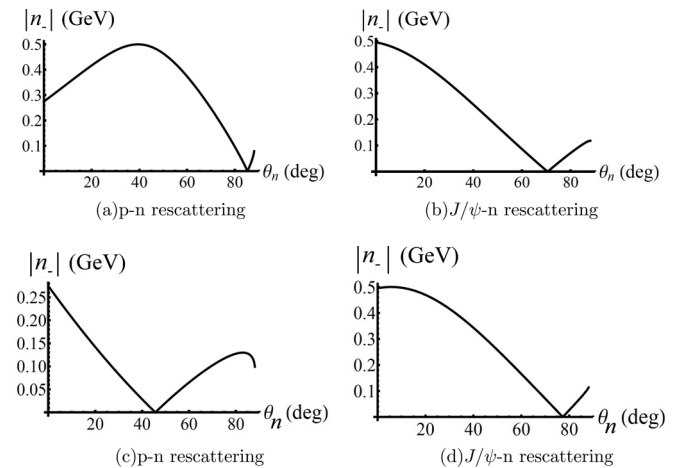

FIG. 15. $|n_-|$ vs θ_n, for photon energy $\nu = 10$ GeV, and $t = -2$ GeV^2. (a) and (b) are for the minus kinematics, (c) and (d) are for the plus kinematics.
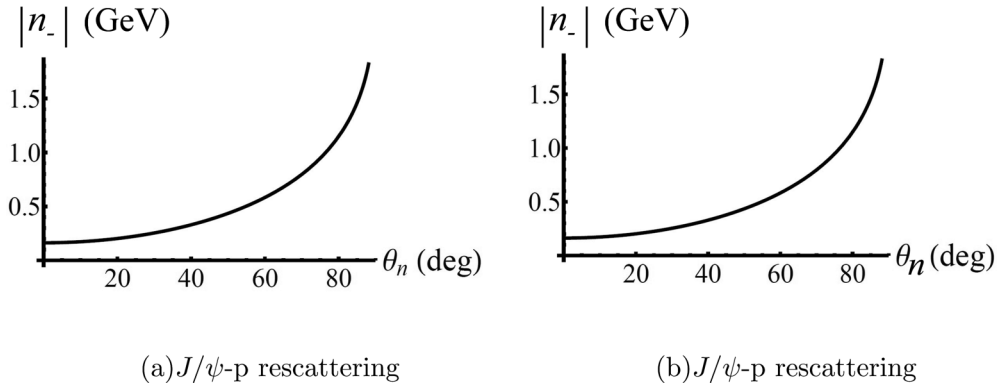
(a) J/ψ-p rescattering

(b) J/ψ-p rescattering

FIG. 16. $|n_-|$ vs θ_n for J/ψ-p rescattering, for photon energy $\nu = 10$ GeV, and $t = -2$ GeV^2. (a) is for the minus kinematics, (b) is for the plus kinematics.

the same set of diagrams as before, shown in Figs. 3 and 4. The impulse diagrams, F_{1a} and F_{1b}, are negligible for these kinematics.

Note that for a given t, p_n, and θ_n, there are two sets of allowed values of the proton and J/ψ momentum $\{\mathbf{p}_p, \mathbf{p}_V\}$; we have called the two sets the "plus" set and the "minus" set. If we define x and z axes as in Fig. 14, with the x component of the neutron momentum always positive, then the plus kinematics is as shown in Fig. 14(a) and the minus kinematics is as shown in Fig. 14(b). For the plus kinematics, p_{px} is negative for all θ_n (while p_{Vx} takes both positive and negative values over the range of θ_n), while for the minus kinematics, p_{Vx} is negative for all θ_n (while p_{px} takes both positive and negative values over the range of θ_n).

Figsures 15 and 16 show graphs of $|n_-|$ vs θ_n for the three different pairs of outgoing particles. Since the value of $|n_-|$ varies greatly with θ_n, the value of the amplitude of the corresponding rescattering diagram varies greatly also, and has a prominent peak at the value of θ_n for which $|n_-| = 0$.

1. Calculation of amplitudes

For the calculation of the amplitudes, the elementary two-body amplitudes $\mathcal{M}^{\gamma V}$ and $\mathcal{M}$ are taken to be of the diffractive form $Ae^{\frac{1}{2}Bt}$ with parameters determined from

existing experimental data. For the J/ψ-nucleon rescattering diagrams, the only available data is from the experiment at SLAC [5] discussed in Sec. IV D. They determined the total J/ψ-nucleon cross section to be $\sigma_{\rm tot}^{J/\psi\, N} = 3.5 \pm 0.8$ mb, which gives via the optical theorem $A_{\rm Vn} = 1.61 \pm 0.4$ GeV^{-4}. The energy of the J/ψ in this experiment was ~ 20 GeV in the Lab frame (nucleon at rest). However, for our kinematics the rescattering of the J/ψ on the nucleon takes place at an energy in the outgoing neutron's rest frame of from 6–10 GeV, which is significantly smaller than in the SLAC experiment; thus the value of $A_{\rm Vn}$ at our energy may be significantly different. Since the entire reason for measuring the cross section for this process is to extract the J/ψ-nucleon scattering amplitude in an energy region where it has not been measured before, we have used several different values of the parameter $A_{\rm Vn}$ in the calculations, from one times the SLAC value up to ten times the SLAC value. Since the total cross section $\sigma_{\rm tot}$ for J/ψ-nucleon scattering goes like $\sqrt{A_{\rm Vn}}$ [Eq. (30)], this corresponds to a range of $\sigma_{\rm tot}$ (which is what was actually measured in the SLAC experiment) of from 1 to ~ 3 times the SLAC value. In Ref. [4], theoretical calculation of the J/ψ-nucleon elastic scattering cross section at threshold yielded 7 mb, which is twice the value measured at the higher energy at SLAC.

The full calculation of the amplitudes must of course include the off-shell parts. If we use the same parametrization
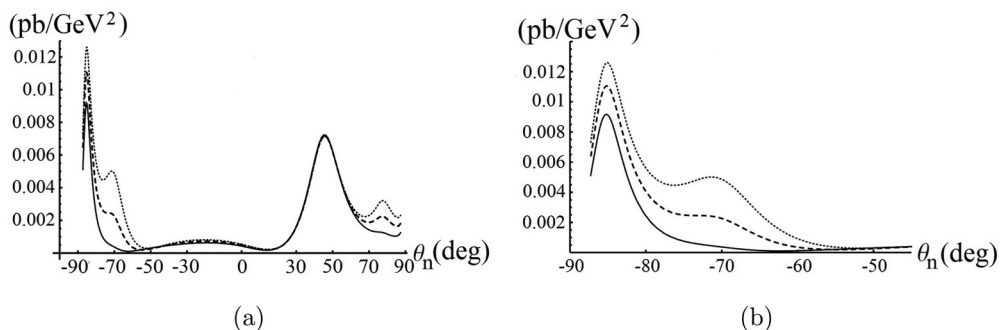

(a)

(b)

FIG. 17. Electroproduction differential cross section vs θ_n, including all diagrams, for photon energy $\nu = 10$ GeV, $Q^2 = 0.5$ GeV^2 and $t = -2$ GeV^2, for three values of $A_{\rm Vn}$: Solid curve: $A_{\rm Vn} = 1.6$ GeV^{-4}. Dashed curve: $A_{\rm Vn} = 8.0$ GeV^{-4}. Dotted curve: $A_{\rm Vn} = 16$ GeV^{-4}. In (a), the large peaks at $\theta_n \simeq 45°$ and $\theta_n \simeq -85°$ are due to $p-n$ rescattering, while the small peaks (or bumps) at $\theta_n \simeq 80°$ and $\theta_n \simeq -70°$ are due to J/ψ-neutron rescattering. (b) shows detail of left half of (a).
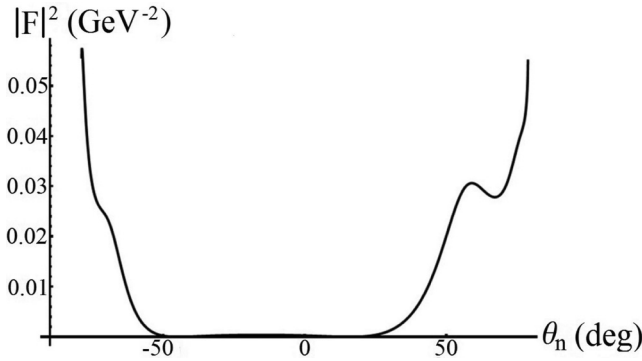
FIG. 18. Amplitude squared vs θ_n, including all diagrams, for $A_{Vn} = 16$ GeV^{-4}, for photon energy $\nu = 9$ GeV and $t = -3$ GeV^2. The peak or bump on either side is due to $p-n$ rescattering, while the peak due to J/ψ-nucleon rescattering is not visible.

of the elementary amplitudes as in the on-shell part, then the off-shell parts were found to be very small compared to the on-shell parts.

The amplitudes F_{2b} and F_{3b}, where the J/ψ is produced on the neutron and then rescattering (of the neutron or J/ψ, respectively) occurs on the proton, are much smaller than F_{2a} and F_{3a}, and do not exhibit the well-defined peaks that F_{2a} and F_{3a} do. Figure 17 shows the eightfold electroproduction differential cross section, Eq. (47), versus θ_n. In that figure, the negative values of θ_n are for the minus kinematics, and the positive values are for the plus kinematics. Graphs are shown for three different values of the J/ψ-neutron elastic scattering parameter A_{Vn}: $A_{Vn} = 1.6$ GeV^{-4} (which is the value determined in the experiment at SLAC), $A_{Vn} = 8.0$ GeV^{-4}, and $A_{Vn} = 16$ GeV^{-4}. It is seen that only if A_{Vn} is of the order of 10 times as large as the previously measured value is there a noticeable peak due to the J/ψ-neutron rescattering, for the plus kinematics. The $p-n$ rescattering peak is much larger than, and close enough to, the J/ψ-neutron rescattering peak that it obscures the J/ψ peak. For the minus kinematics, the same statement holds; in addition, however, the size of the $p-n$ rescattering peak varies (by $\sim$40%) as the value of A_{Vn} is varied. Note also that the position of each of the peaks is simply given by the value of θ_n where the value of the corresponding $|n_-|$ is zero (see Fig. 15).

It's important to note that the peak due to the J/ψ-neutron rescattering isn't observable at lower energies. Figure 18 shows the square of the total amplitude for photon energy of $\nu = 9$ GeV and $t = -3$, for $A_{Vn} = 10 \times 1.6$ GeV^{-4}. On this graph the peak due to $p-n$ rescattering is visible, but there is no visible peak due to J/ψ-neutron rescattering.

B. Conclusion

We have shown here the possibility of measuring the elastic J/ψ-nucleon scattering amplitude for energies significantly smaller than the energy of the only existing data. If the total J/ψ-nucleon cross section $\sigma_{tot}^{J/\psi N}$ at these energies is of the order of 2–3 times the previously measured value, then the differential cross section as a function of θ_n should exhibit well-defined peaks corresponding to on-mass-shell $p-n$ and $J/\psi-n$ rescattering, for virtual photon energy of $\nu = 10$ GeV and four-momentum-transfer-squared $t = (q - p_V)^2 = -2$ GeV^2. However, at lower photon energy (below 9 GeV) the $J/\psi-n$ rescattering peak would not be distinguishable. As it is expected [4] that $\sigma_{tot}^{J/\psi N}$ should increase as the energy decreases, it is not impossible that the lower-energy cross section could be larger than the measured value by a factor of $\sim$2.

VI. CONCLUSION

This paper is concerned with determining information regarding J/ψ-nucleon elastic scattering. As discussed in Sec. IV J, it does not appear possible to measure the J/ψ-nucleon scattering length via production on the deuteron under the kinematic conditions available at JLab. As discussed in Sec. V B, however, it will be possible to extract the J/ψ-nucleon scattering amplitude at higher relative momentum if $\sigma_{tot}^{J/\psi N}$ is large enough.

[1] K. Hafidi *et al.*, JLab Report No. PR12-12-006, 2012 (unpublished).

[2] E. Fuchey *et al.*, JLab Report No. LOI 12-11-002, 2010 (unpublished).

[3] Michael Luke, Aneesh V. Manohar, and Martin J. Savage, Phys. Lett. B **288**, 355 (1992).

[4] Stanley J. Brodsky, and Gerald A. Miller, Phys. Lett. B **412**, 125 (1997).

[5] R. L. Anderson *et al.*, Phys. Rev. Lett. **38**, 263 (1977).

[6] T. Kawanai and S. Sasaki, PoS LATTICE **2010**, 156 (2010).

[7] A. Hayashigaki, Prog. Theor. Phys. **101**, 923 (1999).

[8] A. S. Raskin and T. W. Donnelly, Ann. Phys. (N.Y.) **191**, 78 (1989); **197**, 202 (1990).

[9] J. M. Laget, Phys. Rep. **69**, 1 (1981).

[10] M. L. Perl, J. Cox, Michael J. Longo, and M. N. Kreisler, Phys. Rev. D **1**, 1857 (1970).

[11] H. G. Dosch and E. Ferreira, Phys. Lett. B **576**, 83 (2003).

[12] R. Fiore, L. L. Jenkovszky, V. K. Magas, S. Melis, and A. Prokudin, Phys. Rev. D **80**, 116001 (2009).

[13] Raymond G. Arnold, Carl E. Carlson, and Franz Gross, Phys. Rev. C **21**, 1426 (1980).

[14] B. Gittelman, K. M. Hanson, D. Larson, E. Loh, A. Silverman, and G. Theodosiou, Phys. Rev. Lett. **35**, 1616 (1975).

[15] D. V. Bugg, D. C. Salter, G. H. Stafford, R. F. George, K. F. Riley, and R. J. Tapper, Phys. Rev. **146**, 980 (1966).

[16] J. Beringer *et al.*, Phys. Rev. D **86**, 010001 (2012).

[17] N. Brambilla *et al.*, Eur. Phys. J. C **71**, 1534 (2011).